RESEARCH ARTICLE

NANO · MICRO small
www.small-journal.com

A Photo-induced Cross-Linking Enhanced A and B Combined Multi-Functional Spray Hydrogel Instantly Protects and Promotes of Irregular Dynamic Wound Healing

Guofeng Zhong, Pengkun Lei, Peng Guo, Qin Yang, Yun Duan, Junbo Zhang, Mengyu Qiu, Kaijun Gou, Chen Zhang, Yan Qu,* and Rui Zeng**

Wounds in harsh environments can face long-term inflammation and persistent infection, which can slow healing. Wound spray is a product that can be rapidly applied to large and irregularly dynamic wounds, and can quickly form a protective film in situ to inhibit external environmental infection. In this study, a biodegradable A and B combined multi-functional spray hydrogel is developed with methacrylate-modified chitosan ($CSMA^{1st}$) and ferulic acid (FA) as type A raw materials and oxidized *Bletilla striata* polysaccharide (OBSP) as type B raw materials. The precursor $CSMA^{1st}$-FA/OBSP ($CSOB\text{-}FA^{1st}$) hydrogel is formed by the self-cross-linking of dynamic Schiff base bonds, the CSMA-FA/OBSP (CSOB-FA) hydrogel is formed quickly after UV–vis light, so that the hydrogel fits with the wound. Rapid spraying and curing provide sufficient flexibility and rapidity for wounds and the hydrogel has good injectability, adhesive, and mechanical strength. In rats and miniature pigs, the A and B combined spray hydrogel can shrink wounds and promote healing of infected wounds, and promote the enrichment of fibrocyte populations. Therefore, the multifunctional spray hydrogel combined with A and B can protect irregular dynamic wounds, prevent wound infection and secondary injury, and be used for safe and effective wound treatment, which has a good prospect for development.

1. Introduction

Skin is the body's largest organ to resist the outside world. During the outbreak of the epidemic, many medical personnel suffered serious skin damage due to long-term wearing of protective clothing and disinfection and will also be vulnerable to serious skin damage on the battlefield.[1] In addition, external wounds and chronic skin injuries have secondary infection and chronic inflammation characteristics, so the wound can't heal in a short time. The process of wound healing is extremely complex and includes hemostasis, inflammation, diffusion, remodeling, etc. The orderly progress of each stage can ensure wound healing. After skin injury, its antibacterial ability is greatly reduced, which provides a good condition for bacteria to multiply, which may lead to the formation of infected wounds. At this time, bacteria will cause a large number of inflammatory cell reactions in the wound, thereby slowing down the speed of wound healing. In order to accelerate wound healing, many wound dressings have been designed and manufactured, including hydrogels,[2] microneedles,[3] hemostatic sponges,[4,5] powders,[6] electrospun nanofiber membranes,[7] and other 3D scaffolds similar to extracellular matrix (ECM). In recent years, hydrogels with 3D porous networks have become a research hotspot for wound-healing dressings. Hydrogels are hydrated, 3D networks composed of polymers that can be used to simulate the physical and chemical properties of human skin tissue.[8] Secondly, it can be loaded with biological functional components or modified with good polymers,[9] which can achieve the ideal characteristics of wound dressings to promote wound healing and prevent infection.

Chitosan, a natural polysaccharide, has been widely used in many hydrogels.[10] Chitosan is rich in amino groups that are easy to modify and have certain bactericidal activity.[11] In addition, dextran has the function of triggering the immune system of the body. Oxidized dextran is rich in aldehyde groups and can form self-healing hydrogels with chitosan through the Schiff base reaction. Schiff base cross-linking can not only achieve quickly cross-linked[12,13] but also has dynamic reversibility and a certain

G. Zhong, P. Lei, P. Guo, Q. Yang, Y. Duan, J. Zhang, M. Qiu, C. Zhang, Y. Qu
State Key Laboratory of Southwestern Chinese Medicine Resources
School of Pharmacy
Chengdu University of Traditional Chinese Medicine
Chengdu 611137, China
E-mail: chenzhang_1990@126.com; quyan028@126.com
K. Gou, R. Zeng
College of Pharmacy
Southwest Minzu University
Chengdu 610041, China
E-mail: rzeng@swun.edu.cn
K. Gou, R. Zeng
Key Laboratory of Research and Application of Ethnic Medicine Processing and Preparation on the Qinghai Tibet Plateau
Chengdu 610041, China

The ORCID identification number(s) for the author(s) of this article can be found under https://doi.org/10.1002/smll.202309568

DOI: 10.1002/smll.202309568

responsiveness to the microenvironment, such as the PH change of the wound. Oxidized sodium alginate,[14] Oxidized hyaluronic acid,[15] Oxidized konjac gulcomannnan,[16] and OBSP [17] can react with chitosan through the Schiff base reaction to form self-healing hydrogels. However, these self-healing hydrogels have weak adhesion to wet wounds and limited antibacterial properties.

Based on this, in order to overcome the disadvantages of hydrogels raw materials such as water solubility, antibacterial properties, and poor adhesion, we used CSMA^{1st} as one of the hydrogel frameworks to endow CS with a light curing function. BSP is a natural plant polysaccharide that has been used in ancient times to stop bleeding and detumescence, promote healing, and anti-inflammation.[18] It has good biocompatibility, biodegradability, and a low cost. It has been reported that BSP can be used as a hydrogel material [19,20] and can specifically target macrophages to promote wound healing by inducing macrophage polarization and collagen deposition.[21] FA is a hydroxy-cinnamic acid derivative that is widely found in plants, and is also an active ingredient in many natural plants, and has been widely used in medicine and food fields.[22] To date, FA has been reported to have antibacterial, antioxidant, anti-inflammatory, UV protection, and other effects, and because ferulic acid has a polyphenol structure,[23] it can significantly improve the adhesion of the material.

Here, we propose a novel A/B combined multi-functional spray hydrogel for the treatment of large-area and irregular dynamic wound healing against infection. Type A and type B hydrogels are composed of two biological materials. Type A CSMA^{1st}-FA hydrogel precursor is composed of CSMA^{1st} and FA. Due to the hydrogen bond between CSMA^{1st} and FA, a uniform hydrogel precursor solution can be formed to create a good microenvironment and prevent wound infection. CSMA^{1st} and OBSP can form self-healing hydrogels (CSOB-FA^{1st}) after the Schiff base reaction, which can not only adapt to the deformation during irregular wound movement but also form secondary cross-linking through photo-cross-linking to fit and adhere to the surrounding tissue,[24] providing better wound protection.[25] With the introduction of FA, the hydrogel shows stronger biological adhesion, a good antibacterial effect, and antioxidant ability. Therefore, on the infectious wounds, bottle A is first used for antibacterial and disinfection, and then bottle B is used for wound repair. In addition, the hydrogel could promote the polarization of macrophages to the M2 phenotype, reduce the MPO inflammatory factor, and promote wound healing by rapidly enriching tissue regeneration fibroblasts observed in the wounds of rats and a Bama minipig. In conclusion, the combination of A and B pure natural spray hydrogel dressings has good biological activity, biological safety, simple preparation, abundant raw materials, is easy to carry, and is low cost. It has great application potential in the treatment of large and irregular dynamic wounds in mass casualty accidents.

2. Results and Discussion

2.1. Preparation and Characterization of CSOB-FA Hydrogel

The synthesis process of type A and type B sprayable hydrogels and their application in wound dressing is shown in **Figure 1**. In brief, the three main components of CSMA^{1st}, OBSP, and FA are mixed in the Schiff base reaction to form a preliminary hydrogel network, which is further chemically cross-linked by free radical polymerization of hydrogels under UV–vis light.

BSP is the main active ingredient of the natural plant *Bletilla striata*. The BSP used in this study was extracted and characterized in our laboratory.[26] As shown in the previous characterization, BSP was mainly a hetero-polysaccharide composed of mannose and glucan with a molar ratio of 2.946:1. The total carbohydrate content of BSP was 63.46%, as determined by the phenol-sulfuric acid method. According to HPGPC, the Mw and Mn of BSP were 3.99×10^5 and 7.09×10^4 g mol^{-1}, respectively.

In this work, a photo-cross-linked CS polymer (CSMA^{1st}) (Figure S1A, Supporting Information) and a Schiff base-responsive BSP polymer (OBSP) were designed and synthesized (Figure S1B, Supporting Information).[26] In proton nuclear magnetic resonance (^{1}H-NMR), the methacrylate group was introduced into chitosan by the reaction (MW = 20.0 W kDa, Figure S1C, Supporting Information), and the proton peak of the methacrylate group (—CH=CH$_2$) appeared at 5.34 and 5.65 ppm, confirming the successful coupling. The degree of methacrylation of CSMA^{1st} was 38.88%, as compared with methylene (2.9 ppm). BSP has a clear molecular structure and is currently one of the natural materials used to repair tissue damage. It can obtain other functions through reactions.[27] A new low-intensity aldehyde group peak appeared at 9.28 ppm (Figure S1D, Supporting Information).

Subsequently, the experimental results were verified by Fourier transform infrared spectroscopy (Figure S1E,F, Supporting information). The wave number of BSP and OBSP at 400–4000 cm^{-1} was the typical polysaccharide dominant signal, and the long and broad absorption peak at the wave number of 3399 cm^{-1} was the hydroxyl O—H stretching vibration peak of the polysaccharide. The weak absorption peak with wave numbers of 2927 cm^{-1} is the stretching vibration peak of C—H, and the wave numbers of 1151, 1062, and 1031 cm^{-1} show the presence of pyranose. An enhanced carbonyl (C=O) stretching vibration absorption peak was observed at 1735 cm^{-1}, which indicated that part of the hydroxyl group was changed to an aldehyde group after the oxidation of BSP. In the infrared spectrum of CSMA^{1st}, the out-of-plane bending vibration peak of C—H on C=C is at 838 cm^{-1}. In addition, compared with CS, the stretching vibration absorption peak of —NH$_2$ at 1598 cm^{-1} are weaken, while the characteristic absorption peaks of amide II and III bands appeared at 1550 and 1234 cm^{-1}, respectively. The appearance of the C=C absorption peak, the disappearance of the amino absorption peak, and the formation of the amide bond absorption peak also indicate the acylation of the amino groups on MA and CS. By comparing the infrared spectra of OBSP, CSMA^{1st} FA, CSOB, and CSOB-FA hydrogels, it can be seen that the symmetry vibration peak of C=O belonging to OBSP at 1735 cm^{-1} was significantly weakened, and the absorption peak of C=N appeared at 1643 cm^{-1}, indicating that a Schiff base reaction occurred between the —CHO group of OBSP and the —NH$_2$ group of chitosan, that is, a Schiff bond was formed. For FA, the characteristic peak of —COOH at 1695 cm^{-1} in CSOB-FA was significantly weakened, indicating that the electrostatic interaction between —COOH of FA and —NH$_2$ of CSMA resulted in the blue shift of the vibrational peak of the CSOB protonated amino group, suggesting that the hydrogel cross-linking reaction was successful. Significant changes

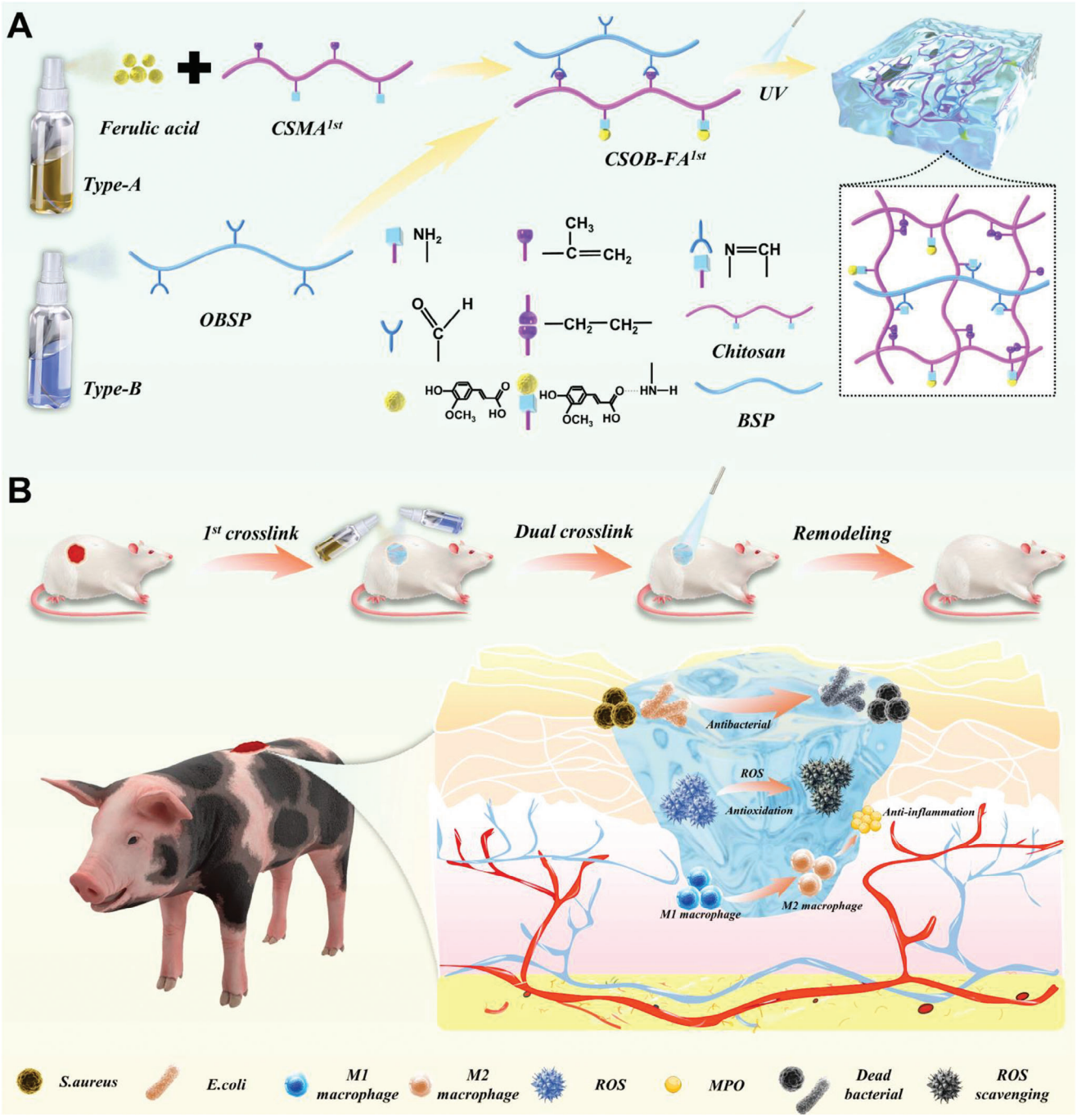

Figure 1. A multifunctional all-natural A and B combination spray hydrogel as an immunomodulatory dressing for infectious wound healing. A) Schematic diagram of preparation of type A and type B combined spray hydrogel CSOB-FA. B) Immunoregulatory effect of CSOB-FA composite hydrogel on bacterially infected wound healing.

were observed in the infrared spectral region at 1500–1600 cm^{-1}, associated with the C═C unsaturated groups, which underwent chemical reactions after UV irradiation, and a gradual decrease in the re;ative strength associated with the C═C was observed before and after UV irradiation, confirming effective photo-crosslinking of hydrogels.[28] A tube inversion test was used to further confirm gel formation (Figure S1G, Supporting Information). Both the $CSMA^{1st}$ -FA solution and the OBSP solution showed some fluidity before the addition of OBSP. With the addition of OBSP, the $CSMA^{1st}$ -FA/OBSP mixture began to hydrogel, but at this time, the $CSOB\text{-}FA^{1st}$ hydrogel was the first step of cross-linking. The hydrogel was soft and did not flow with the tube, but the hydrogel had some deformation. After optical crosslinking, it does not tilt with the inverted tube and does not deform. The

CSMA^{1st}-FA/OBSP cross-linking reaction was successfully performed as described above to prepare the hydrogel CSOB-FA. To further understand the structural changes of the hydrogels, the crystal changes of the raw materials used (BSP, OBSP, and CSMA^{1st}) and the prepared hydrogel samples (CSMA, CSOB, and CSOB-FA) were investigated by XRD (Figure S2A,B, Supporting Information). OBSP and CSMA^{1st} are typical polymers with low crystallinity. In the range of 10–80 θ, compared with the XRD patterns of the hydrogels CSMA, CSOB, and CSOB-FA, the crystallinity of the hydrogels in this range is smaller, which can be compared by the intensity of the peaks, which may be caused by the network interpenetration of the hydrogel. This may have interfered with the degree of crystallization, so XRD was able to show that the crystallinity of the hydrogel was reduced due to the cross-linking of the H and Schiff bonds of the hydrogel, which also reduced the intensity of the XRD peaks.

2.2. Physical Characteristics of the Hydrogel

The pore-like structure of the hydrogel can conduct gas exchange for the wound, which is beneficial to the supply of nutrients and oxygen and lays a certain foundation for promoting wound healing[29] Taking CSMA, CSOB, and CSOB-FA as references, the morphology of the hydrogel was studied by SEM. According to the SEM figure (**Figure** 2A), compared with CSMA and CSOB hydrogels, CSOB-FA had a smaller pore size and a uniform distribution, which was mainly due to the different cross-link density in the hydrogel network. Therefore, CSOB-FA will have a tighter network structure.

In situ drug delivery is not limited to in situ spray administration; it can also be delivered by in situ injection. To demonstrate the diversity of delivery routes for type A and type B spray gels, we used a single-channel syringe to inject the hydrogel to visualize "CDUTCM 2023" (Figure 2B-i),[30] mixing the hydrogel precursor. After the hydrogel was formed, it was immediately transferred into a common syringe for in situ injection, and we verified that the hydrogel was also very good in water (Figure 2B-ii), which showed that the hydrogel had good injectability and could be used for in situ drug delivery through multiple channels. Then we put the hydrogel CSMA^{1st}-FA and OBSP precursor into the spray bottle and then sprayed them into three different shapes hydrogels ("✿", "♥" and "★") at the same time (Figure 2B-iii). After the light curing forming the gel, it shows the adaptability of the hydrogel spray to different shapes.[31] It turns out that the hydrogel spray can be adapted to large areas and irregular shapes of wounds.

The storage modulus G' and loss modulus G" of CSMA, CSOB, and CSOB-FA hydrogels were evaluated by rheological experiments (Figure 2C–G) and shows the sol-to-gel dynamic process. The storage modulus (G') was higher than the loss modulus (G") for all samples, indicating hydrogel formation, where G' values were generally above G" at frequencies ranging from 0.1 to 100 rad s^{-1}. In addition, the storage modulus of CSOB and CSOB-FA hydrogels was higher than that of CSMA single-network hydrogels. The CSOB hydrogel after photo-cross-linking was more stable than the CSOB^{1st} hydrogel after photo-cross-linking before photo-cross-linking. This may be due to the formation of a dynamic Schiff bond between CSMA^{1st} and OBSP, while CSOB is more stable after photo-cross-linking. The G" values of CSMA, CSOB^{1st}, and CSOB-FA^{1st} are higher than G' at high oscillation frequencies. The CSOB-FA hydrogel showed better stability and rigidity after photo-cross-linking. After 4 consecutive alternating repeated cycles, the value of G' was still larger than G", indicating the self-healing behavior of the CSOB-FA hydrogel (Figure 2H).[32] At the same time, the viscosity of the different hydrogels was measured by a rheometer (Figure 2I,J). The viscosity of CSOB-FA is higher than that of CSMA and CSOB hydrogels, which may be due to the enhanced adhesion of FA due to the phenolic hydroxyl group in FA. After lighting, the viscosity of the hydrogel is stronger, while the adhesion of CSOB has little change after photo-cross-linking, which may be due to the denser cross-linking of CSOB-FA hydrogel after photo-cross-linking. This leads to the formation of more intermolecular hydrogen bonds, which increases its viscosity.[33]

To verify the self-healing results of CSOB-FA in the rheological experiment, the self-healing ability of the hydrogel was evaluated by macroscopic self-healing experiments [34] (Figure 2K; Figure S3A, Supporting Information). The cylindrical hydrogel samples were divided into two parts, and then both parts were placed at room temperature, and the hydrogel was allowed to heal without any external intervention. After healing, the two ends were clamped with tweezers and stretched in opposite directions, respectively, and the cracks of the hydrogel were not broken. The dynamic Schiff base bond between the amino group in CSMA and the aldehyde group in OBSP endows the hydrogel with excellent self-healing properties, while the phenolic hydroxyl group in FA may help the hydrogel achieve better self-healing.

The mechanical properties of the hydrogel can be easily changed by changing the lighting time to meet the needs of the hydrogel for different tissues.[35] In order to characterize the mechanical properties of CSOB-FA hydrogels with different cross-linking times, compression tests were performed on the samples under different cross-linking conditions of 10, 15, and 30 s. As shown in **Figure** 3A,B, the stress-strain curves show that the rigidity of the hydrogel improves with increasing cross-linking time. With the delay of light time, the compression modulus of CSOB-FA hydrogel increased significantly (5 s CSOB-FA: 2.9 ± 0.19 kPa, 15 s CSOB-FA: 7.04 ± 1.58 kPa, 30 s CSOB-FA: 8.84 ± 1.34 kPa). A high degree of cross-linking is conducive to the formation of strong hydrogels, but too much cross-linking can lead to the relative fragility of the hydrogels. In order to obtain hydrogels with appropriate strength and elasticity, a cross-linking time of 15 s was selected as the optimization condition. At the same cross-linking time, the compressive modulus of CSOB-FA hydrogel (11.94 ± 2.76 kPa) and CSOB (16.60 ± 3.51 kPa) was significantly lower than that of the single network (Figure 3C,D) and the single component CSMA (37.39 ± 9.31 kPa). It may be due to the existence of a dynamic Schiff bond and an H bond in the double-network hydrogels, which leads to the mechanical properties of the gels not being as good as those of the single-network hydrogels with CSMA radical cross-linking. However, the single-network hydrogel with free polymerization reaction has the characteristics of too high relative fragility, which may not be suitable for protecting wounds from dynamic changes. The bearing capacity of physiological soft tissues is in the range of 10–200 kPa.[36] In general, the compression modulus of CSOB-FA hydrogel is suitable as a scaffold for cell proliferation, migration, and differentiation in physiological soft tissues.

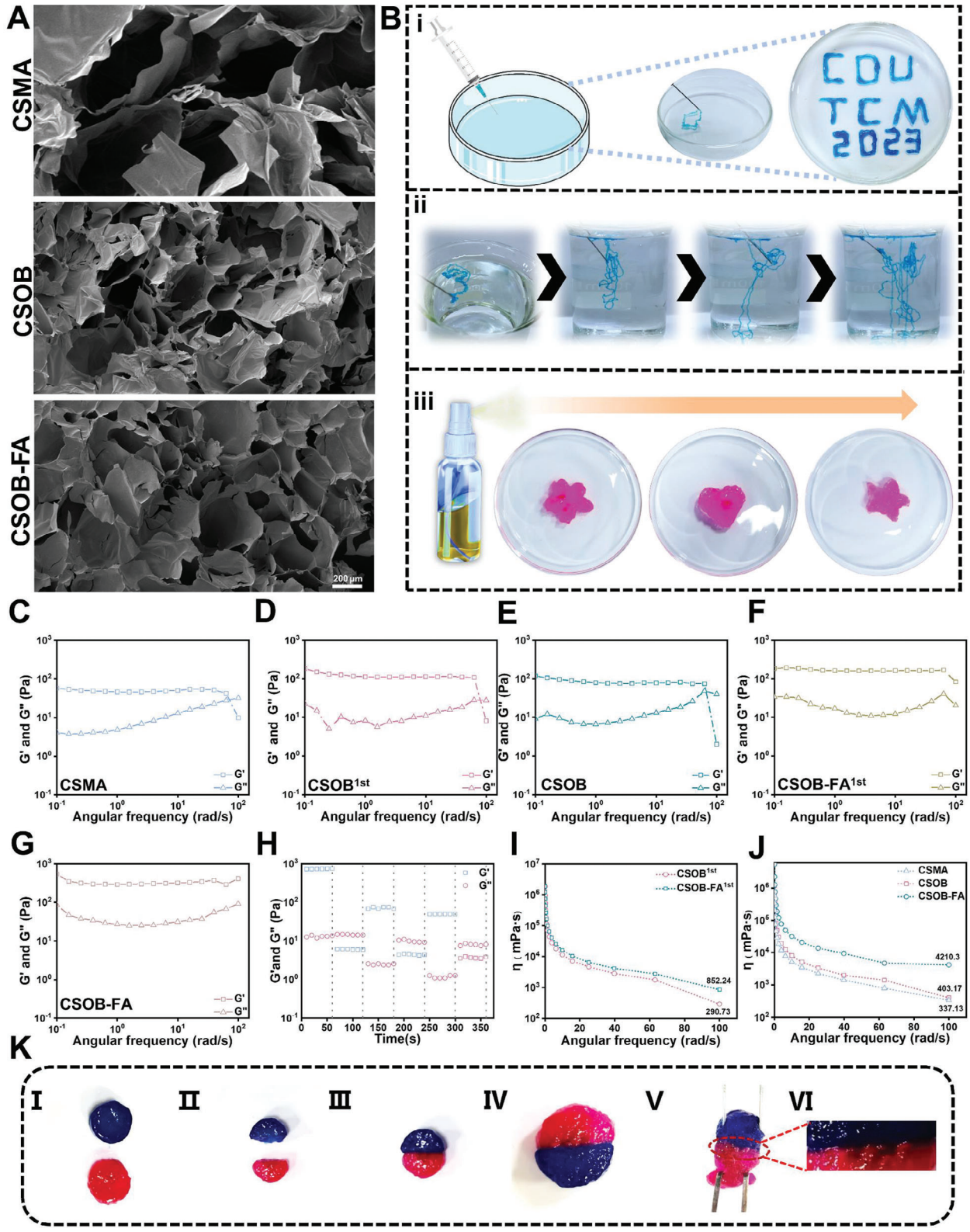

Figure 2. Preparation method of the hydrogel raw material and characterization of basic properties of hydrogel. A) SEM photo of the hydrogel. Scale bar = 200 μm. B) i) Injectability of hydrogels. ii) Morphological diagram of hydrogel injected into water. iii) Shape adaptation of the spray hydrogel. C) Rheogram of CSMA hydrogel. D) Rheogram of CSOB^{1st} hydrogel without UV curing. E) Rheogram of CSOB hydrogel after UV curing. F) Rheogram of CSOB-FA^{1st} without UV-curing hydrogel. G) Rheogram of UV-cured hydrogel CSOB-FA. H) assay of shear healing ability of CSOB-FA hydrogel. I) Viscosity plots of CSOB^{1st} and CSOB-FA^{1st} hydrogels before lighting. J) Viscosity diagrams of CSMA, CSOB, and CSOB-FA hydrogels after lighting. K) A macroscopic picture of self-healing hydrogel.

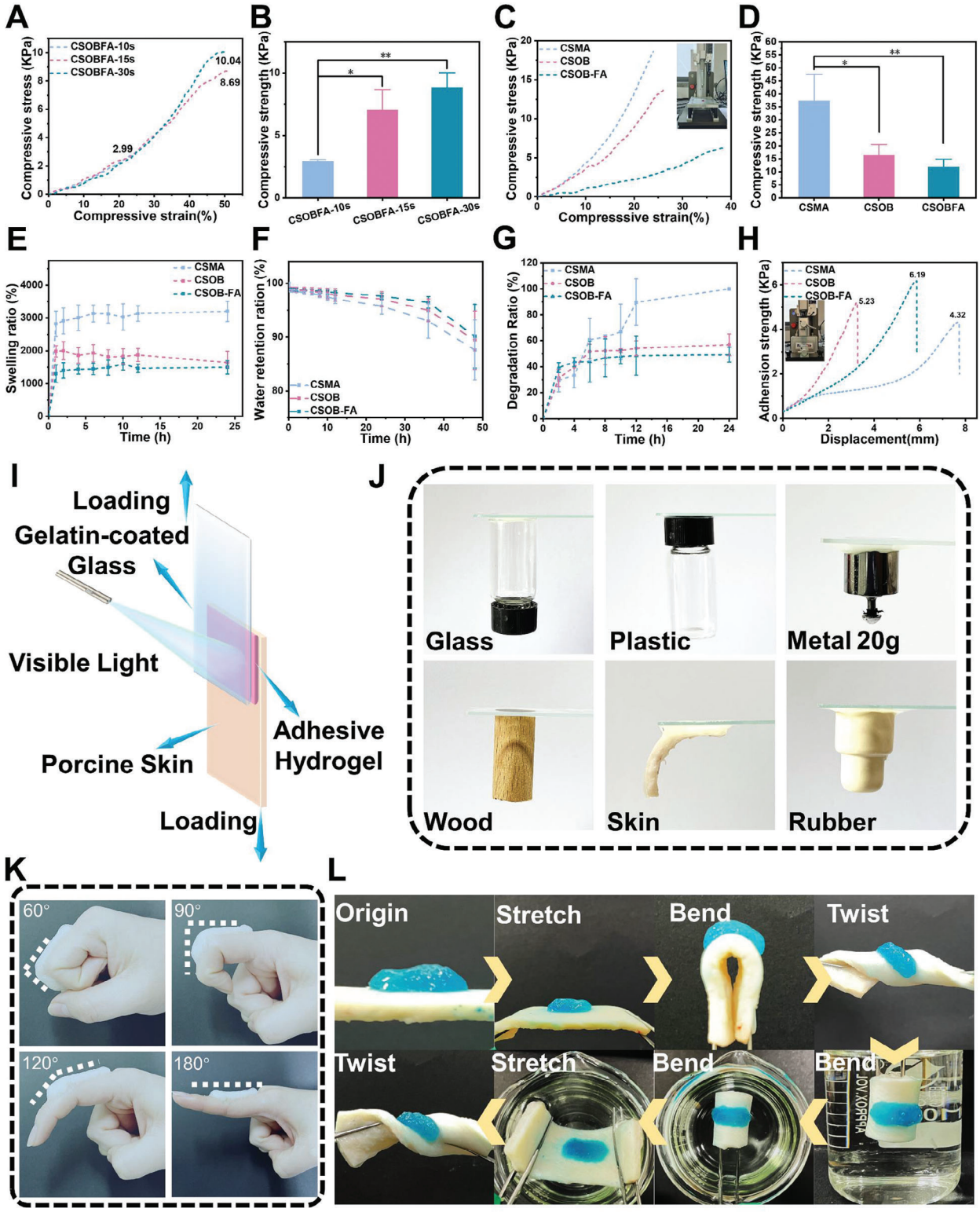

Figure 3. Physical and chemical properties of the prepared hydrogels. A) Stress–strain curves of CSOB-FA hydrogel after UV cross-linking for 10, 15, and 30 s. B) Compression modulus of CSOB-FA hydrogel after UV cross-linking for 10, 15, and 30 s (n = 3). C) Stress-strain curves of CSMA, CSOB, and CSOB-FA hydrogels. D) Compression modulus of CSMA, CSOB, and CSOB-FA hydrogels (n = 3). E) Swelling of the hydrogel (n = 4). F) Water retention capacity of hydrogel (n = 5). G) Degradation rate of the hydrogel after 24 h of degradation (n = 6). H) Stress-strain curve of the adhesion ability of hydrogel pigskin. I) Schematic representation of the pigskin adhesion tensile test. J) Adhesion diagram of hydrogel on different materials. (K) The adhesion of hydrogel in dynamic finger joints. L) Distorted pictures of the hydrogel on the table and after immersion in water. Data represent mean ± SD; $^{*}p$ <0.05, $^{**}p$ <0.01.

The swelling rate can be used to evaluate whether the hydrogel can provide wet conditions for the wound and protect the application site from external physical compression.[37,38] Therefore, when hydrogels are used for wound healing, low-swelling hydrogels may be more beneficial for wound healing. The lowest swelling rate of CSOB-FA was ≈14 times its dry weight, which was 1/2 of the single-network CSMA hydrogel. Hydrogels can avoid reduced flexibility due to high swelling rates, which may cause rupture and degradation of the hydrogel before wound healing, leading to secondary wound trauma [39] (Figure 3E).

The water retention property of hydrogels is that water is retained in the hydrogel network for a long time, which can maintain the relative humidity in the wound.[40] In wet wounds, epithelial layer formation is faster because epithelial cells are more likely to proliferate in wet wounds, thereby protecting and promoting wound healing. Water evaporation experiments were performed to evaluate the water retention ability of the hydrogels. The experimental results are shown in Figure 3F. The water content in all the tested hydrogels decreased with time. The CSMA hydrogel showed the fastest and largest rate of water loss, followed by CSOB, while the CSOB-FA hydrogel showed the slowest and smallest rate of water loss throughout the experiment. All the hydrogels could maintain more than 85% water content after 48 h. However, the rate and amount of water evaporation varied among groups, which depended on the tightness of the network in the hydrogels, further indicating that the CSOB-FA hydrogel network had a tighter structure.

To evaluate the degradation of the hydrogel, we immersed the hydrogel in a lysozyme solution (2%, w/v).[41,42] CSOB-FA degraded slowly (Figure 3G), which was suitable for chronic wound healing. The degradation rate was 49.27 ± 5.75% after 24 h of incubation. Because CSMA-FA and OBSP are intertwined, their degradation rate is slower than that of CSOB. At the same time, CSMA is degraded faster in an enzymatic solution, which is not suitable for long-term wounds. Therefore, CSOB-FA is more suitable for wound healing with a suitable degradation ability to maintain a suitable environment for wound healing.

Hydrogel dressings that completely adhere to irregular wound tissue can prevent wound infection, promote skin wound closure, and provide a microenvironment conducive to wound tissue repair. The adhesion properties of the hydrogels were evaluated by a lap shear test. When OBSP and FA were introduced, respectively, the adhesion strength of the hydrogel was improved (Figure 3H). The gelatin-rich glass plate and fresh pig skin were used as the test surfaces to simulate human skin tissue, as shown in Figure 3I. This result also confirmed the rheological complex viscosity experiments, which demonstrated a significant increase in the adhesion of CSOB-FA. It has been reported that the adhesion strength of hydrogels depends on the adhesion force on the surface and the cross-linking density within the gel, which is enhanced by groups such as H bond, aldehyde, and phenolic hydroxyl groups.[43] Therefore, CSOB-FA hydrogel has better tissue adhesion ability, sufficient adhesion groups to ensure enhanced interface adhesion, and denser cross-linking density inside. The adhesion of CSOB-FA hydrogel to different matrix materials was also photographed (Figure 3J). Interestingly, CSOB-FA hydrogel has good adhesion to glass, plastic, metal, wood, skin, rubber, and other materials and can withstand a certain weight. Besides, the strong adhesion property provides the hydrogel with the ability to be suitable for dynamic wounds with high-frequency motion. Therefore, photos of the hydrogel adhered to the knuckle, skin, and stretched and twisted in water were taken, as well as the photos of CSOB-FA adhered and stretched (Figure 3K,L; Figure S3B, Supporting Information). The results of torsional stretching and torsional stretching in water showed that the hydrogel had good toughness, and no rupture occurred. These experimental data demonstrate that the good adhesive properties of hydrogels are beneficial for providing a stable connection for dynamic wounds and dressings.

2.3. Antibacterial Activity of Hydrogels

The antibacterial activity of chitosan is derived from the positive charge carried by its protonated amino group, while the bacterial biofilm carries a negative charge, so the positive charge reacts with the negative charge, leading to bacterial death. The in vitro antibacterial effects of CSMA, CSOB, and CSOB-FA were evaluated against *S. aureus* and *E. coli* (**Figure 4**A). Compared with the control group, the CSOB group had more colonies, indicating poor antibacterial activity, which may be due to the reduced presence of amino groups after CSMA reacted with OBSP and thus showed poor antibacterial effect (Figure 4B). Both the CSMA and CSOB-FA groups showed significantly fewer bacteria. They showed excellent antibacterial activity against *S. aureus* and *E. coli*, with bacterial survival rates of less than ≈3% after 24 h of co-culture with Staphylococcus aureus and Escherichia coli. However, the bacterial survival rate of the CSOB group was all above 25% (Figure 4C), indicating that the existence of a Schiff bond between OBSP and $CSMA^{1st}$ could form gel, and at the same time, the amount of amino group in $CSMA^{1st}$ was reduced, so its antibacterial property was low. With the addition of FA, the antibacterial ability of CSOB hydrogel was significantly improved. In order to further observe the antibacterial effect of the gel, we cultured *S. aureus* and *E. coli* with different groups of hydrogels and observed their antibacterial effect by scanning electron microscopy (Figure 4D). In the control group, *S. aureus* and *E. coli*, which were normally grown, were spherical and rod-shaped, respectively, with smooth surfaces because they did not have antibacterial substances. So the bacteria can multiply and reproduce normally. In the CSOB-FA and CSMA groups, the cell membranes of the two bacteria precipitated certain contents, accompanied by obvious shrinkage and deformation, while in the CSOB group, a small amount of bacteria deformation, contraction and the outflow of bacterial contents were observed. The results showed that the prepared CSOB-FA hydrogel had good broad-spectrum antibacterial activity against bacteria such as *S. aureus* and *E. coli* under the synergistic effect of FA.

2.4. Cell proliferation, Migration and Biocompatibility

Safety is the first standard used in medicine, so whether the hydrogel has good cell compatibility is very important for the application of hydrogels in biomedicine. CCK-8 and direct contact experiments were used to evaluate the cytotoxicity of CSMA, CSOB, and CSOB-FA hydrogels. Under confocal fluorescence microscopy, a large number of living cells with green spindle

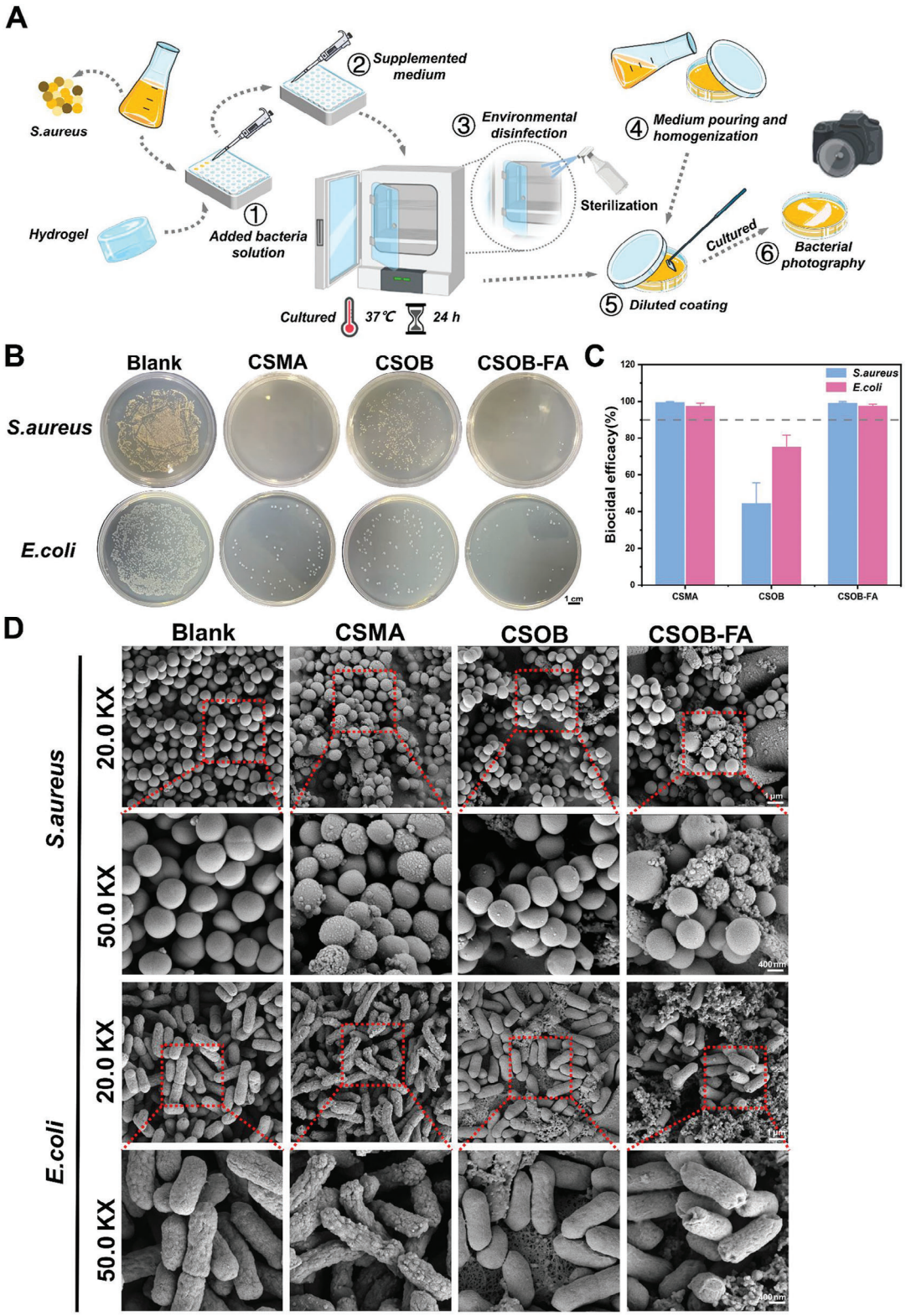

Figure 4. Antibacterial ability of hydrogels. A) Schematic diagram of the antibacterial experiment on hydrogel. B) Representative plot of representative colony agar after co-culture of hydrogel with *S. aureus* and *E. coil*. Scale bar = 1 cm. C) Antibacterial rate of hydrogel (n = 3). (D) SEM images of bacteria in the bacterial invasion assay. Scale bar = 1 and 400 μm.

morphology could be observed, and the cell morphology was normal after 48 h (**Figure 5A**). There were almost no dead cells, and it was exciting that they continued to show a state of cell proliferation from day 0. The hydrogel at different concentrations showed good cell compatibility (more than 80%) at 24 and 48 h, and cell proliferation was produced (Figure 5B,C), indicating that this series of hydrogels had no cytotoxicity and produced satisfactory cell compatibility. The hydrogel culture medium was co-cultured with the cells for 48 h. Although CSMA, CSOB, and CSOB-FA all had good cytocompatibility, in general, the CSOB-FA hydrogel had significant differences compared with the other two groups ($P < 0.05$).

Cell migration is one of the processes in wound healing, and the cell migration experiment (Figure 5D) was used to verify whether the hydrogel has a pro-healing function.[44] Therefore, in the cell migration experiment (Figure 5E), with the increase in hydrogel treatment time, CSOB-FA showed a more satisfactory degree of cell migration than the CSMA and CSOB groups. At 48 h, the cell migration rate of the CSOB-FA group was more than 85%, while the cell migration rate of the blank group was only ≈26.4%, that of CSMA was only ≈46.3%, and that of CSOB was 60.6%. There was a significant difference in the scratch width between the CSOB-FA group and the other groups ($P < 0.001$) (Figure 5F). Therefore, CSOB-FA hydrogel has the function of wound healing. In the wound, macrophages are difficult to convert from pro-inflammatory M1 to M2 macrophages, which will prolong the inflammatory phase of the wound and reduce the rate of wound healing. Specific biomaterials may regulate their differentiation. The RAW264.7 cell line was used to evalate the polarization effect of hydrogel, and flow cytometry was used to detect the transformation level of macrophages in each group (Figure S4A, Supporting Information).[45,46] Cells were incubated with CSMA, CSOB, and CSOB-FA hydrogels. The results showed that CSOB-FA hydrogel effectively promoted the transformation of macrophages from M1 to M2 types. In the Figure S4B,C, the CSOB-FA group had the best effect in promoting macrophage transformation.

In addition, wound dressings are inevitably in contact with blood,[47] and hemolysis is considered to be one of the important indicators to evaluate the biocompatibility of biomaterials,[48] so the biocompatibility of hydrogels is evaluated by hemolysis tests. All hydrogels did not cause any obvious hemolysis after incubation, and the absorbance was significantly different from that of the positive group ($P < 0.001$) (Figure 5G). The hydrogel groups did not show any significant difference compared with the negative group, indicating that these hydrogels had good blood compatibility.[49] Together, these results indicate that CSOB-FA hydrogels are biocompatible and non-hemolytic and support cell adhesion, growth, and proliferation.

2.5. Antioxidant Activity of Hydrogel

A large amount of ROS is produced in the skin wound environment, and with the large accumulation of ROS, the wound will show a state of chronic oxidative stress. Wound dressings containing antioxidants are effective in scavenging ROS and contributing to chronic wound healing. FA is reported to be a good antioxidant,[50] which is usually encapsulated in various carriers to prevent its oxidation and achieve sustained release when used for wound repair. Therefore, in order to evaluate the good antioxidant effect of CSOB-FA hydrogel on the bacterially infected wound, the in vitro antioxidant performance of CSOB-FA hydrogel was studied by a DPPH free radical scavenging experiment. With the increase in hydrogel concentration, DPPH free radical scavenging efficiency was continuously improved. When the hydrogel concentration increased to 4 mg mL^{-1}, the DPPH free radical scavenging rate was greatly enhanced (Figure 5H). Compared with the CSMA and CSOB groups, there were significant differences ($P < 0.001$).

2.6. In vivo Hemostasis of Hydrogel

In large irregular, dynamic wounds, persistent bleeding after debridement should not be ignored, and effective hemostasis is a prerequisite for effective wound healing (Figure S4A,B, Supporting Information).[51] A mouse hepatic hemorrhage model was used to evaluate the hemostatic ability of CSOB-FA hydrogel compared with CSMA (69.73 ± 5.54 mg) and the blank group (130.63 ± 17.69 mg). The blood loss of CSOB (20.35 ± 8.49 mg) and CSOB-FA (19.2 ± 8.60 mg) was significantly reduced ($P < 0.001$) (Figure. S4C, Supporting Information). To further evaluate the hemostatic ability of the hydrogel, the clotting time of the sample after contact with blood was tested.[52] It was found that the complete clotting time of the sample alone was ≈6 min, a stable blood clot was formed after ≈4.2 min of contact with CSMA gel (Figure. S4D, Supporting Information), and the best clotting effect of CSOB-FA was 3.5 min. Compared with the CSOB and CSMA groups, there were statistically significant differences ($P < 0.05$) (Figure S4E, Supporting Information). Compared with the other two groups, the BCI index of the CSOB-FA group was significantly different ($P < 0.001$)[53] (Figure S4F; Supporting Information).

2.7. Healing of the Infected Wound

In order to evaluate the wound healing effect of CSOB-FA hydrogel in vivo, a SD rat bacterially infected skin defect model was established, and a full-thickness skin defect model of rats infected with Staphylococcus aureus was used to evaluate the healing ability of the hydrogel on the infected wound. The experimental procedure is shown in **Figure 6A**. It is obvious that the CSOB-FA hydrogel has almost completely healed. And the healing is very fast; it can be almost completely healed in 13 days. For the blank and CSMA groups, the wound was still clearly visible, and the wound was still obvious compared with the CSOB group (Figure 6B). These results all indicate that the CSOB-FA hydrogel has better wound healing ability (Figure 6C,D), which may be due to the good ability of the OBSP component in the hydrogel to promote tissue repair. At the same time, FA helps to provide antibacterial capacity to accelerate the healing of infected wounds. (Figure S6 Supporting Information).

The first step of skin healing is mainly skin epithelialization tissue regeneration.[54] Thus, the wound healing was further evaluated by H&E staining and Masson staining, and the results are shown in Figure 6E. Eight days after treatment, the skin gaps of

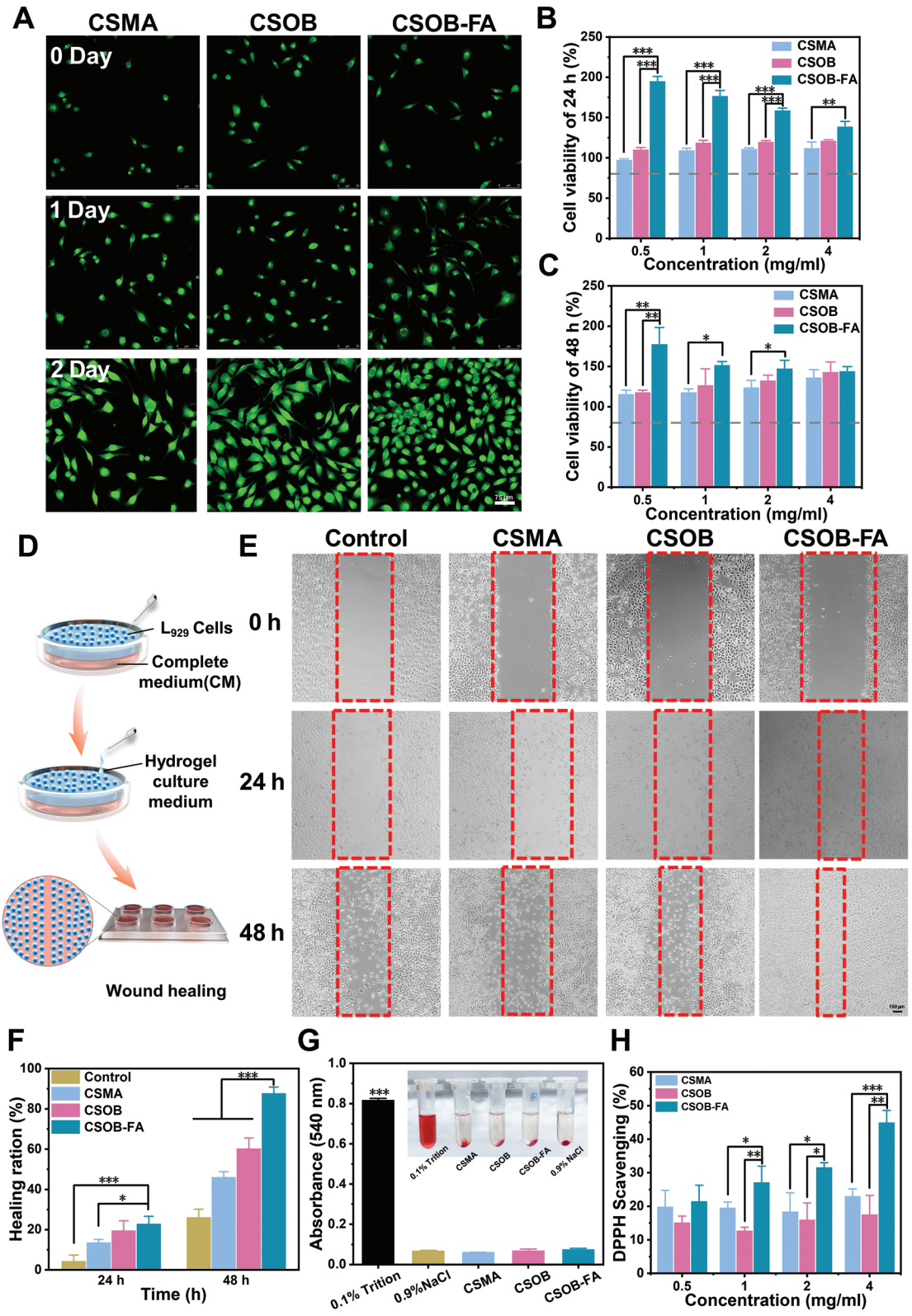

Figure 5. Properties of hydrogel cell proliferation, cytotoxicity, cell migration, biocompatibility, and antioxidant activity. A) Staining diagram of L929 cells after co-culture of cells and hydrogel. Scale bar = 75 μm. B) Viability of L929 cells cultured in hydrogel for 24 h. C) Cell viability of L929 cells after 48 h of hydrogel culture. D) Schematic diagram of the L929 cell migration assay. E) Cell scratch migration experiment diagram. F) Quantitative plot of cell migration after hydrogel culture of cells (n = 3). (G) Hemolytic absorbance of 1% Triton X-100, CSMA, CSOB, and CSOB-FA in the positive control and 0.9% NaCl solution in the negative control (n = 3). H) DPPH radical scavenging activity of the hydrogel (n = 3). Data represent mean ± SD; $^{*}p$ <0.05, $^{**}p$ <0.01, and $^{***}p$ <0.001.

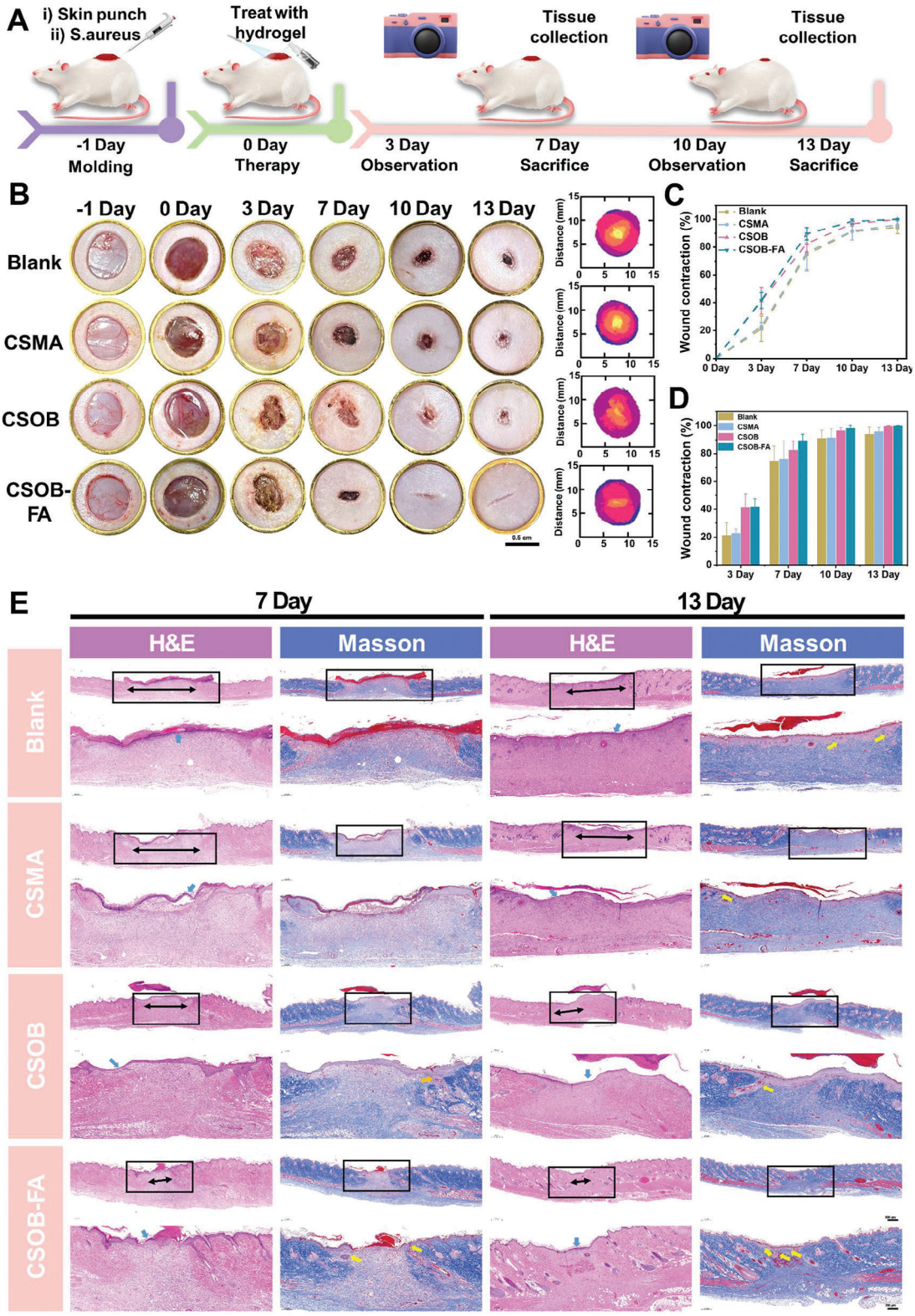

Figure 6. Treatment of bacterially infected wounds with hydrogels. A) Experimental protocol for bacterially infected skin wounds. B) Representative images of wound healing treated with different gels. Scale bar = 0.5 cm. C,D) Statistical curves and graphs of wounds. E) Images of H&E staining and Masson staining of wounds in different treatment groups on days 7 and 13. The blue arrow represents the area of epithelization. The yellow arrow represents the newly formed dermis. Scale bar = 500 and 200 μm.

the CSMA group and the CSOB group were blurred, while the gaps of the CSOB-FA group had been reduced (Figure S7A, Supporting Information), and there was a large amount of new granulation tissue. On day 13, the epidermal structure of the skin in each group was complete and gradually thickened (Figures S5B and S7B,C, Supporting Information), but large areas of new granulation tissue were still observed in the CSMA and CSOB groups, while significant improvement was observed in the CSOB-FA group, with multiple hair follicles and new blood vessels. The density and thickness of collagen fibers were the largest. The results showed that type A and type B multifunctional spray gels could improve bacterial wound infection and promote wound healing.

In the process of infectious wound healing, bacterial infection can prolong the inflammatory period of the wound, thereby affecting the healing rate of the whole wound. Existing reports show that BSP and FA can reduce the level of wound inflammation,[21,55] induce the transformation of M1 macrophages into M2 macrophages, and effectively accelerate the wound healing period. In this study, CD86 and CD206 were used as M1 and M2 macrophage markers to evaluate the level of inflammation on the 7th day of the infected wound (**Figure** 7A). In order to test the anti-inflammatory ability of hydrogel, MPO^+ was measured as a representative of inflammatory factors (Figure 7B). This study showed that CD86 expression was decreased and CD206 expression was up-regulated, indicating a trend of macrophage transformation from M1 to M2 macrophages (Figure 7C,D), which was also consistent with previous reports. FA was shown to have a synergistic effect with OBSP on enhancing the transformation of M1 to M2 macrophages. The results of MPO^+ showed that MPO^+ in the blank group was significantly higher than that in the other treatment groups and slightly higher in the CSMA group, while both CSOB and CSOB-FA showed low inflammation (Figure 7E). This indicates that the wounds in the blank group were still in the inflammatory phase and were unable to transition to the next phase, which reduced the rate of wound healing.

In order to simulate human skin,[56] an animal trauma model of a Bama miniature pig weighing 11.6 kg was established. The deep trauma wounds were distributed on both sides of the pig's spine. The animals were fed under normal conditions and observed at different time points. The experimental process is shown in Figure 8A (Videos S1 and S2, Supporting Information). The hydrogel in the CSOB-FA group has better wound healing ability. However, the size of the tissue around the wound was still clearly visible, and there was no sign of contraction in the blank group, and the scab had been decrusted at 14 days, while the blank control was still able to decrube at 21 days, indicating that the CSOB-FA gel was more effective in promoting wound healing (Figure 8B). H&E and Masson showed that the hydrogel skin gap in the CSOB-FA group was significantly reduced (Figure 8C; Figure S7D, Supporting Information), the epidermis had healed completely (Figure S7E, Supporting Information), the granulation tissue was significantly thickened (Figure S7F, Supporting Information), and the collagen density increased. The results showed that CSOB-FA hydrogel not only promoted wound healing in small animals but also promoted wound healing in large animals with dynamic wounds. Although the healing time may be longer, this may be due to the deep wound depth and large wound area, so the skin of the miniature pig was approximately complete after 21 days. At the same time, the hydrogel had completely covered the wound, and the area of the blood scab was completely larger than the initial area of the skin wound due to the combination of the gel with the blood scab during healing, indicating that the gel could completely adhere to the wound tissue and fall off with the blood scab. Therefore, the specific healing rate could not be determined.

3. Conclusion

In this study, a photo-cross-linked CSMA and OBSP were fabricated by reactive methacrylate groups and selective oxidation. A spray hydrogel combined with A ($CSMA^{1st}$-FA) and B (OBSP) was prepared by dynamic Schiff bond cross-linking. A simple one-step UV–vis light cross-linking curing hydrogel (CSOB-FA) was used around the tissue. CSOB-FA hydrogel is porous, biodegradable, and has regulating mechanical properties. It can regulate the wound environment without adding other therapeutic agents. Compared with single hydrogel, CSOB-FA hydrogel can effectively improve bacterial infection, cell migration, proliferation, and adhesion in vitro. Moreover, in vivo evaluation confirmed the effectiveness of CSOB-FA hydrogel in promoting dynamic infectious wound healing, regulating macrophage polarization, and proper collagen deposition during wound healing, with good biocompatibility and hemostatic properties. In summary, CSOB-FA hydrogels show great potential for chronic wound treatment, are easy to carry, and have good therapeutic potential in irregular, dynamic wounds.

4. Experimental Section

Preparation of $CSMA^{1st}$: According to literature reports,[57] the experimental method was improved. 1 g of chitosan (CS, Mw = 20.0w kDa, Macklin, Shanghai, China) powder was dissolved in 100 mL of 1% acetic acid solution, stirred evenly until dissolved, then 1.0 mL of methacrylic anhydride (MA) solution was added, stirred at room temperature for 24 h, and put into a dialysis bag. After the reaction, distilled water was cyclically dialyzed (Mw: 3.5–8.0 kDa) at room temperature for 3 days, freeze-dried, and finally $CSMA^{1st}$ solid was obtained.

OBSP Preparation: OBSP was prepared according to the method previously described for the experiment. In brief, 3.00 g of BSP (previously prepared in the laboratory (Supporting Information) was precisely weighed and added to 50.0 mL of deionized water, prepared with sodium iodate as an oxidizing agent, stirred evenly until dissolved, and then, according to the previous laboratory report, according to the molar ratio of BSP to $NaIO_4$ of 0.4, the ratio of BSP to NaIO4 was calculated. 1.44 g of $NaIO_4$ was precisely weighed and added to 50.0 mL of deionized water, and BSP solution and $NaIO_4$ solution were mixed and stirred for 12 h. 2 mL of ethylene glycol was added for 2 h to ensure that the reaction was complete, and the reacted system was placed into a dialysis bag (Mw: 3.5 kDa) and dialyzed by circulation with distilled water for 3 days at room temperature. Finally, OBSP solid was obtained by freeze-drying.

Preparation of Hydrogel: Prepare 200 mg of OBSP and 200 mg of $CSMA^{1st}$ solid dissolved in 10 mL of deionized water solution to prepare 2% (w/v) OBSP and 2% (w/v) $CSMA^{1st}$ precursor solution, respectively. Then 0.8% (w/v) FA (Mw = 194.18, Aladdin, Shanghai, China) and 0.2% (w/v) lithium phenyl (2,4,6-trimethylbenzoyl) phosphonate (LAP, Mw = 154.16, Macklin, Shanghai, China) were added to the $CSMA^{1st}$ precursor solution, the $CSMA^{1st}$-FA solution was obtained after mixing evenly, and then $CSMA^{1st}$ solution, $CSMA^{1st}$-FA solution, and OBSP solution were loaded into 5 mL spray bottles (75 µL per drive) and mixed according to

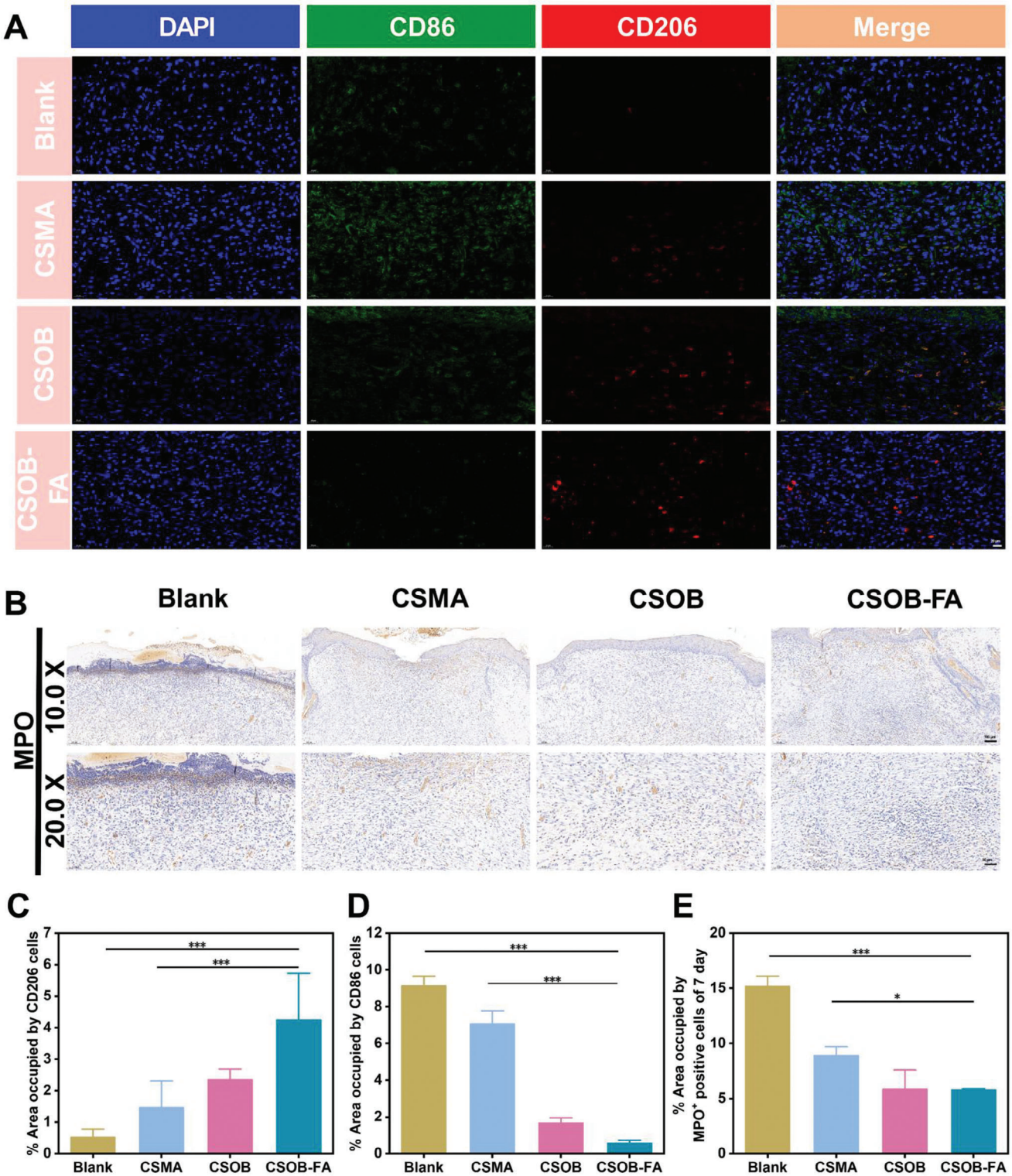

Figure 7. Immunohistochemical diagram of infected skin wounds on day 7. A) Macrophage polarization maps of skin wounds of different hydrogel treatment groups and control groups at day 7. M1 and M2 macrophages (CD86, green; CD206, red). Nuclei (DAPI, blue). Scale bar = 20 μm. B) Representative image of MPO^+ in the wound. Scale bar = 100 and 50 μm. C) The percentage of M2 macrophages (n = 3). D) The proportion of M1 macrophages (n = 3). E) MPO^+ neutrophils after day 7 (n = 3). Data represent mean ±SD; $^*P < 0.05$ and $^{***}P < 0.001$.

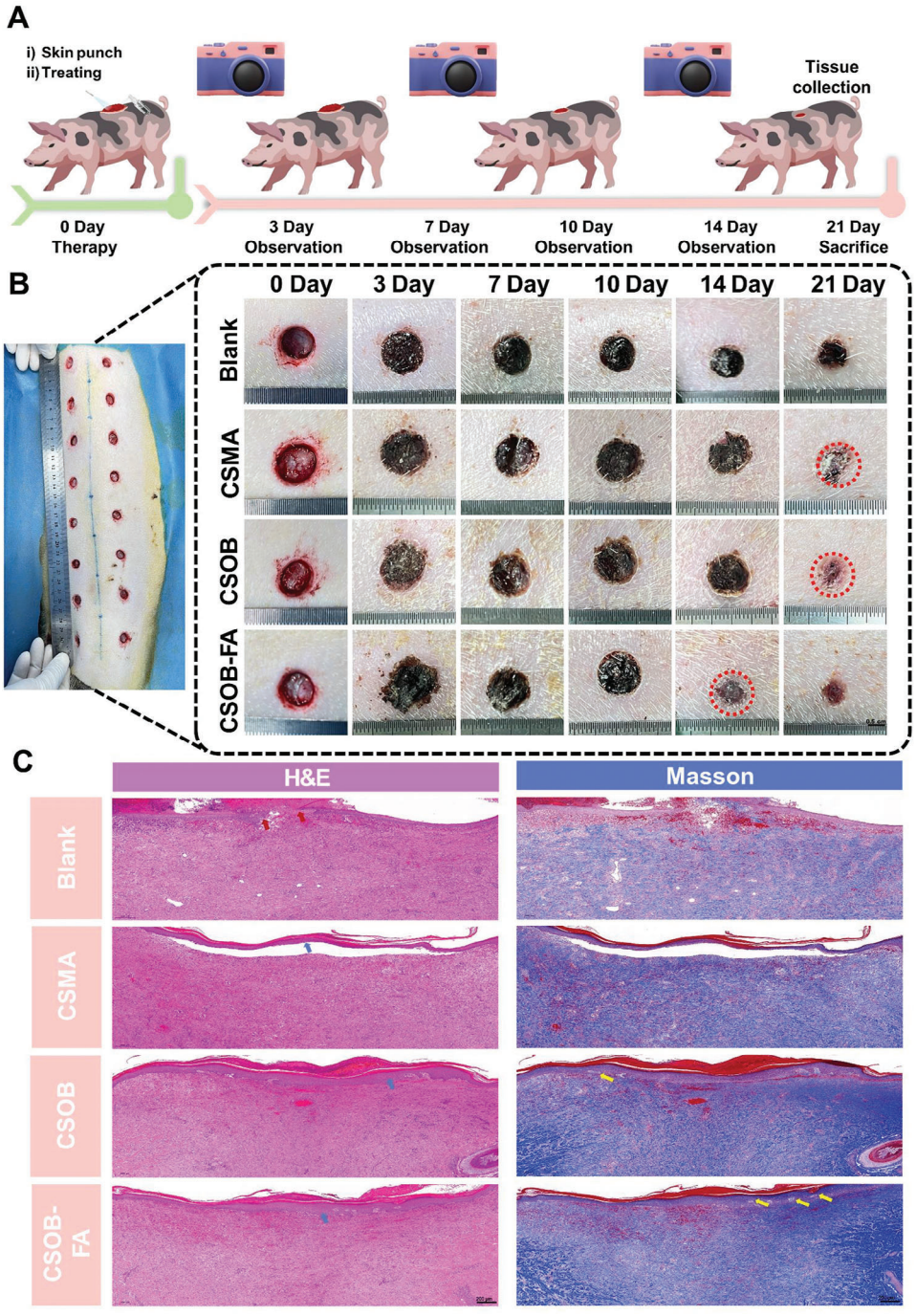

Figure 8. Hydrogel treatment of Bama miniature pig wounds. A) Experimental treatment protocol for skin wounds. B) Representative images of wound healing after gel treatment. Scale bar = 0.5 cm. C) Images of H&E staining and Masson staining of wounds in different treatment groups on day 21. The red arrow represents the unhealed area. The blue arrow represents the area of epithelization. The yellow arrow represents the newly formed dermis.

the ratio of spray times: 1:1. First, CSMA^{1st} solution, CSOB^{1st} hydrogel, and CSOB-FA^{1st} hydrogel were formed, and then the hydrogel was cured by UV–vis light (405 nm) to form CSMA, CSOB, and CSOB-FA hydrogel.

SEM Scanning Electron Microscopy: The hydrogels were characterized by SEM (Axio Imagerm2 EVO10, Germany). Before examination, the hydrogel samples were freeze-dried, and the hydrogel samples were used with a sputter gold plating machine (CRESSINGTON108) for 40 s to minimize the charging effect and observe the morphology of the different hydrogel cross-sections.

Hydrogel Injectability, Jetting, and Shape Adaptability: methylene blue staining was added to the CSOB-FA hydrogel after formation, stirred evenly, and immediately transferred to a syringe with a 16-gauge needle. The injectability of the hydrogel was evaluated by injecting the word

"CDUTCM 2023" into the hydrogel. In addition, two precursor solutions, CSMA^{1st}-FA and OBSP, were sprayed into different shapes of the membranes to evaluate their shape adaptability.

Macroscopic Self-Healing Ability of the Hydrogel: At room temperature, the disc-shaped hydrogel was cut into two parts from the middle and separated by a certain distance, then the two parts were placed in place and waited for a certain time until the two parts of the hydrogel were polymerized again. After that, the ends of the hydrogel were removed and lifted for stretching, and the healed hydrogel was kept in suspension. All photographs of the hydrogel were taken.

Rheological Property: The rheological properties of hydrogels were evaluated by using a rheometer (MCR72, Anton Paar). The hydrogels CSMA, CSOB1st, CSOB, CSOB-FA1st and CSOB-FA were prepared at room temperature with a diameter of 30 mm and a height of 3.0 mm respectively. The energy storage modulus (G′) and loss modulus (G″) of each hydrogel sample and the viscosity of each hydrogel sample were determined using a rheometer in the oscillating frequency range of 25 °C and 0.1∼100 rad s^{-1}. The hydrogel self-healing property was also determined by 3ITT method.

Mechanical Properties of Hydrogels: The mechanical properties of CSMA, CSOB, and CSOB-FA hydrogels, as well as the effect of lighting time, were evaluated by the compression of the hydrogels. Briefly, the hydrogel was prepared as a cylinder with a diameter of 14 mm and a height of 1.2 cm. The hydrogels were then tested using a texture analyzer (Rapid TA$^+$, Shanghai Tengba Instrument Technology Co., Ltd.) at a speed of 1 mm S^{-1}.

Swelling Properties: The swelling rate of each hydrogel sample was determined by the following method: Briefly, once formed, the hydrogels were lyophilized and weighed (Wd). Subsequently, the hydrogel samples were placed in 10 mL of PBS at room temperature. From time to time, the water on the surface of the hydrogel was filtered and weighed (Wt). Finally, the weight of the hydrogel no longer changes, and the equilibrium swelling state is reached. The swelling rate of the hydrogel at different times was calculated by the following equation:

$$\text{Swelling ratio} = (Wt - Wd)/Wd \times 100\% \quad (1)$$

Wd and Wt represent the weights of the dried and expanded gels at different time points, respectively.

Water Retention Experiment: Each sample was placed at 37 °C, and the relative humidity in the environment was maintained at 72.06 ± 0.32% with saturated sodium chloride. Samples were taken out at the determined experimental point, then weighed, and finally lyophilized. Water retention rate is defined as follows:

$$\text{Water retention rate } (\%) = W_0 - W_t/W0 \times 100\% \quad (2)$$

W_0 and W_t represent the gel weight at different time points and the weight of the initial water that removed the dry weight of the gel after lyophilization, respectively.

Bond Properties: The bond strength of the hydrogel was tested by a lap shear test; briefly, fresh pig skin was cut into rectangles (50 × 20 mm^2) and placed in distilled water. Subsequently, the CSOB-FA hydrogel precursor solution was prepared. The precursor solution of the hydrogel was transferred to the subcutaneous tissue of the porcine skin, where excess surface water was removed using filter paper. Then, the other glass plate was evenly coated with gelatin dissolved in PBS (20%, w/v), the adhesive area was 10 × 20 mm^2, and the lighting time was controlled at 30 s. The bond strength was measured with a texture analyzer (Rapid TA$^+$, Shanghai Tengba Instrument Technology Co., Ltd.) at a tensile rate of 1 mm s^{-1}. CSMA and CSOB hydrogels were used as control groups. The suitability of the hydrogel for dynamic wounds was evaluated by attaching the hydrogel to human finger joints. In addition, the adhesion properties of the hydrogel with different materials were evaluated by attaching the hydrogel to glass bottles, plastic, metal (20 g), wood, pig skin, and rubber at room temperature.

Antibacterial In Vitro: In vitro antibacterial activity of the hydrogel against Gram-negative Escherichia coli (*E. coli*, CMCC (B) 44 102) and Gram-positive Staphylococcus aureus (*S. aureus*, ATCC 25 923) was tested by the plate colony counting method. Bacteria were inoculated in liquid medium (tryptophan soy broth, TSB) and kept at 37 °C for 48 h to prepare bacterial solutions (10^8 CFU mL^{-1}). Before the addition of bacteria, the hydrogel (50 mg) was placed in four sets of three parallel wells in each set were set in a 48-well plate. The first group was placed without hydrogel as a control group, and the remaining three groups were placed sequentially with CSMA, CSOB, and CSOB-FA. 200 µL of the above bacterial solution and 800 µL of liquid medium were added to the respective wells and continued at 37 °C for 24 h. Subsequently, the bacterial broth from the same group was removed and mixed, and subsequently, the bacterial broth from the same group was removed and mixed, serially diluted with sterile saline, and spread on plate counting agar (PCA). Finally, all plates were incubated at 37 °C for 24 h and photographed using a camera, and colonies were counted using Image J software. The bacteria were then collected and fixed with a glutaraldehyde solution (2.5%, w/v) for 8 h, followed by gradient elution with ethanol. The bacteria were then lyophilized and stored for subsequent scanning electron microscopy.

Cytotoxicity Assessment: To study the cytotoxicity of hydrogels, 200 mg of sterile hydrogel (immersed in 50 mL of complete medium and incubated at 37 °C for 24 h) was used to obtain hydrogel extracts for cell culture at concentrations of 4, 2, 1, and 0.5 mg mL^{-1}, respectively. L929 cells were seeded in 96-well plates at a density of 5000 cells $well^{-1}$ and cultured for 24 h in a CO2 incubator. After that, the hydrogel extracts were co-cultured with the cells for 24 and 48 h, 10 µL Cell Counting Kit-8 (CCK-8, Macklin, Shanghai, China) reagent was added to each well, and the plates were incubated for an additional 30 min. The absorbance (OD) was read through a microplate reader. Relative cell viability was calculated by the equation:

$$\text{Relative cell viability } (\%) = ((ODs - ODb)\ /\ (ODc - ODb)) \times 100\% \quad (3)$$

ODs is the average absorbance of the sample (hydrogel) group; ODc is the average absorbance of the control group. ODb is the mean absorbance of the blank group.

Cell Migration Assay: To evaluate the effect of the hydrogel on cell migration, L929 cells in the logarithmic growth phase were collected and seeded at a concentration of 3 × 10^6 cells $well^{-1}$ in a six-well plate. After occupying 80% of the bottom space of the plate under 5% CO_2 and 37 °C, the wound was simulated by drawing a straight line on the cell surface through the 200 µL tip of a sterile pipetter (outer diameter ≈0.8 mm). The cell debris was washed three times with PBS (pH = 7.4), and 1 mL of Live Dead Cell Staining was added to the control group kit, Dulbecco's Modified Eagle's Medium (DMEM, Thermofisher, America) complete medium. In the hydrogel group, 1 mL of hydrogel co-culture medium was added, and the cell migration to the wound was observed under an optical microscope. The migration of cells was monitored by photographing at 24 h and 48 h.

$$\text{Cell migration rate (wound healing rate) } (\%) = (T0 - Tn)\ /T0 \times 100\% \quad (4)$$

where T0 is the initial scratch area and Tn is the intercellular area at different times.

Antioxidant Activity: The antioxidant activity of the hydrogel was assessed by a DPPH radical scavenging assay. Briefly, 40.0 mg of CSOB-FA pre-hydrogel solution was dispersed in 10.0 mL of pure water. The above dispersion was diluted to 4, 2, 1, and 0.5 mg mL^{-1}, respectively, and added to DPPH solution (0.08 mg mL^{-1}), and pure water was added to a final volume of 1 mL. After the reaction at 37 °C for 2 h, the absorbance at 517 nm was measured by UV–vis spectroscopy. DPPH degradation was calculated using the following formula:

$$\text{DPPH clearance } (\%) = (A_0 - A_n)\ /A_0 \times 100\% \quad (5)$$

A_0 is the absorbance of the final solution dispersed by the 0 µL sample, and A_n is the absorbance of the final solution dispersed by different volumes of sample.

Biocompatibility: The biocompatibility of the hydrogel is evaluated by an in vitro hemolysis test. 1.0 g of the hydrogel sample is weighed, added to 10 mL of normal saline, and immersed in a biochemical incubator at 37 °C for 48 h. Blood from the auricular vein of New Zealand white rabbits is centrifuged at 2000 rpm for 10 min to isolate red blood cells and then washed three times with normal saline. Purified red blood cells were diluted with normal saline to obtain a suspension of red blood cells (5%, v/v). A saline negative control and a 0.1% Triton X-100 positive control were selected for this study. A 200 µL RBC suspension was prepared and mixed with 100 µL hydrogel suspension and 700 µL 0.9% NaCl solution as the experimental group. Cultures were incubated for 1 h at 37 °C, the tubes were centrifuged at 1500 rpm for 5 min to absorb the supernatant, and absorbance is measured at 540 nm.

Wound Healing in Rats: Nine male Sprague-Dawley rats weighing 180–250 g were selected as the experimental subjects. The rats were randomly divided into a control group and an experimental group. After anesthesia, the hair on the back was removed, and a circular wound with a diameter of 8 mm was made on the back of the rats with a biopsy punch. The bacterial infection wound model was established by adding 50 µL of bacterial suspension (Staphylococcus aureus, 10^8 CFU mL^{-1}) to the wound and covering the wound with a sterile closed PU membrane for 24 h. The three hydrogels, CSMA, CSOB, and CSOB-FA, were then sprayed and cross-linked, followed by UV curing for 15 s. The animals were randomly divided into four groups, and in the control group, CSMA hydrogel, CSOB hydrogel, and CSOB-FA hydrogel were applied, respectively. The digital images of the wounds were collected on the 3rd, 7th, and 13th days after operation and measured by Image J software.

$$\text{The percentage of healed area} = [A0 - A(3, 7, 13)/A0] \times 100\% \quad (6)$$

A0 and A (3,7,13) represent the unhealed areas on days 0 and 3,7,13, respectively.

Subsequently, the corresponding skin tissue samples were taken for H&E staining, Masson staining, macrophage polarization, and MPO^+ inflammatory factor analysis. All mice were purchased from SPF (Beijing, China) Biotechnology Co., Ltd., and the ambient temperature was 23 ± 2 °C. The relative humidity was 55 ± 5%. 12 h light-dark cycle. The animals had unrestricted access to tap water and standard rat food throughout the trial, and their beds were changed three times a week. All animal experiments were approved by the Society for the Care of Laboratory Animals, Chengdu University of Traditional Chinese Medicine, according to the recommendations for the handling and use of laboratory animals issued by the National Institutes of Health.

Wound healing in pigs: an 11.4 kg Bama miniature pig was selected. After anesthesia, the hair on the back of the Panamax miniature pig was removed and disinfected, and a full-thickness skin wound with a depth of 8 mm and a size of 10 mm was created using a biopsy punch. The three hydrogels, CSMA, CSOB, and CSOB-FA, were then sprayed and cross-linked, followed by UV curing for 15 s. The animal wounds were randomly divided into 4 groups, which were treated with the control group, CSMA hydrogel, CSOB hydrogel, and CSOB-FA hydrogel, respectively. Digital images of the wound were collected at 3, 7, 14 and 21 days after the operation. Skin tissue samples from day 21 were subsequently taken for H&E and Masson staining analysis. Bama-type miniature pigs were from Senwei (Chengdu, China) Laboratory Animal Co., LTD. The ambient temperature was 22 ± 1°C. The relative humidity was 60 ± 1% with a 12 h light-dark cycle. During the whole experiment, the animals were provided with drinking water and food twice a day. According to the recommendations for the handling and use of laboratory animals issued by the National Institutes of Health of the United States, all animal experiments were approved by the Laboratory Animal Care Society of Chengdu Senwei Laboratory Animal Co., Ltd. (Ethics number: DOSSYLL20230720001).

Statistical analysis: Origin 2021 was used for one-way ANOVA, and the data were presented as mean ± SD. Tukey's post hoc test was used to assess whether there were significant differences. The statistically significant difference was defined as $P < 0.05$.

Supporting Information

Supporting Information is available from the Wiley Online Library or from the author.

Acknowledgements

This work was supported by the National Natural Science Foundation of China (82374303), the Natural Science Foundation of Sichuan Province (2023YFS0348 and 2023NSFSC1768, 2022NSFC0373), the China Postdoctoral Science Foundation (2021M690488 and 2023T160071), The Southwest Minzu University Research Startup Funds (RQD2023005), The Central Guidance on Local Science and Technology Development Fund of Sichuan (23ZYZYTS0155), Innovation Team and Talents Cultivation Program of National Administration of Traditional Chinese Medicine (ZYYCXTD-D-202209).

Conflict of Interest

The authors declare no conflict of interest.

Author Contributions

G.F.Z. contributed to methodology, data curation, and writing – original draft. P.K.L. contributed to the investigation and formal analysis. P.G. and Q.Y. contributed to the validation. Y.D., J.B.Z., and M.Y.Q. contributed to visualization. K.J.G., C.Z., Y.Q., and R.Z., contributed to conceptualization, writing – review and editing, funding acquisition, and project administration.

Data Availability Statement

Research data are not shared.

Keywords

A and B combined spray hydrogel, Healing of infected wound, Irregular dynamic wound

Received: October 22, 2023
Revised: November 22, 2023
Published online:

[1] W. Guan, C. Gong, S. Wu, Z. Cui, Y. Zheng, Z. Li, S. Zhu, X. Liu, *Adv. Mater.* **2023**, *36*, 2306589.
[2] N. Annabi, D. Rana, E. Shirzaei Sani, R. Portillo-Lara, J. L. Gifford, M. M. Fares, S. M. Mithieux, A. S. Weiss, *Biomaterials* **2017**, *139*, 229.
[3] P. Zhou, S. Zhao, C. Huang, Y. Qu, C. Zhang, *Int. J. Biol. Macromol.* **2022**, *205*, 511.
[4] Q. Yan, X. Long, P. Zhang, W. Lei, D. Sun, X. Ye, *Carbohydr. Polym.* **2022**, *293*, 119696.
[5] Q. Zhang, C. Qi, H. Wang, X. Xiao, Y. Zhuang, S. Gu, Y. Zhou, L. Wang, H. Yang, W. Xu, *Carbohydr. Polym.* **2019**, *226*, 115304.
[6] X. Zhang, L. Jiang, X. Li, L. Zheng, R. Dang, X. Liu, X. Wang, L. Chen, Y. S. Zhang, J. Zhang, D. Yang, *Small* **2021**, *18* ,2101699.
[7] G. Zhong, M. Qiu, J. Zhang, F. Jiang, X. Yue, C. Huang, S. Zhao, R. Zeng, C. Zhang, Y. Qu, *Int. J. Biol. Macromol.* **2023**, *234*, 123693.
[8] S. Cascone, G. Lamberti, *Int. J. Pharm.* **2020**, *573*, 118803.

[9] S. H. Park, H. J. Ju, Y. B. Ji, M. Shah, B. H. Min, H. S. Choi, S. Choi, M. S. Kim, *Small* **2021**, *17*, 2103244.
[10] X. Wang, P. Xu, Z. Yao, Q. Fang, L. Feng, R. Guo, B. Cheng, *Front. Bioeng. Biotechnol.* **2019**, *7*, 1.
[11] X. Li, F. Jiang, Y. Duan, Q. Li, Y. Qu, S. Zhao, X. Yue, C. Huang, C. Zhang, X. Pan, *Int. J. Biol. Macromol.* **2023**, *229*, 654.
[12] Y. Du, L. Li, H. Peng, H. Zheng, S. Cao, G. Lv, A. Yang, H. Li, T. Liu, *Macromol. Biosci.* **2019**, *20*, 1900303.
[13] L. Zhou, L. Zhou, C. Wei, R. Guo, *Carbohydr. Polym.* **2022**, *291*, 119558.
[14] M. Zhang, X. Qiao, W. Han, T. Jiang, F. Liu, X. Zhao, *Carbohydr. Polym.* **2021**, *266*, 118100.
[15] W. Tan, T. Long, Y. Wan, B. Li, Z. Xu, L. Zhao, C. Mu, L. Ge, D. Li, *Carbohydr. Polym.* **2023**, *312*, 120824.
[16] C. Zhang, X. Yang, W. Hu, X. Han, L. Fan, S. Tao, *Int. J. Biol. Macromol.* **2020**, *149*, 31.
[17] L. Yang, Z. Han, C. Chen, Z. Li, S. Yu, Y. Qu, R. Zeng, *Mater. Sci. Eng., C* **2020**, *117*, 111265.
[18] C. Zhang, Y. He, Z. Chen, J. Shi, Y. Qu, J. Zhang, *Evid. Based Complementary Altern. Med.* **2019**, *2019*, 1.
[19] J. Chen, H. Zhou, D. Xie, Y. Niu, *Chin. Med.* **2021**, *16*, 131.
[20] S. Jakfar, T.-C. Lin, Z.-Y. Chen, I. H. Yang, B. A. Gani, D. S. Ningsih, H. Kusuma, C.-T. Chang, F.-H. Lin, *Int. J. Mol. Sci.* **2022**, *23*, 12019.
[21] N. Xu, Y. Gao, Z. Li, Y. Chen, M. Liu, J. Jia, R. Zeng, G. Luo, J. Li, Y. Yu, *Chem. Eng. J.* **2023**, *466*, 143173.
[22] D. Li, Y.-x. Rui, S.-d. Guo, F. Luan, R. Liu, N. Zeng, *Life Sci.* **2021**, *284*, 119921.
[23] G. Li, Y. Y. Lee, X. Lu, J. Chen, N. Liu, C. Qiu, Y. Wang, *Int. J. Biol. Macromol.* **2022**, *219*, 333.
[24] Y. Qian, Y. Zheng, J. Jin, X. Wu, K. Xu, M. Dai, Q. Niu, H. Zheng, X. He, J. Shen, *Adv. Mater.* **2022**, *34*, 2200521.
[25] Y. J. Fu, Y. F. Shi, L. Y. Wang, Y. F. Zhao, R. K. Wang, K. Li, S. T. Zhang, X. J. Zha, W. Wang, X. Zhao, W. Yang, *Adv. Sci.* **2023**, *10*, 2206771.
[26] C. Chen, P. Zhou, C. Huang, R. Zeng, L. Yang, Z. Han, Y. Qu, C. Zhang, *Carbohydr. Polym.* **2021**, *273*, 118557.
[27] X. Yue, S. Zhao, M. Qiu, J. Zhang, G. Zhong, C. Huang, X. Li, C. Zhang, Y. Qu, *Carbohydr. Polym.* **2023**, *312*, 120831.
[28] I. C. Carvalho, H. S. Mansur, *Mater. Sci. Eng. C* **2017**, *78*, 690.
[29] Y. Yu, P. Li, C. Zhu, N. Ning, S. Zhang, G. J. Vancso, *Adv. Funct. Mater.* **2019**, *29*, 1904402.
[30] S. Bian, Z. Zheng, Y. Liu, C. Ruan, H. Pan, X. Zhao, *J. Mater. Chem. B* **2019**, *7*, 6488.
[31] S. Tavakoli, H. Mokhtari, M. Kharaziha, A. Kermanpur, A. Talebi, J. Moshtaghian, *Mater. Sci. Eng., C* **2020**, *111*, 110837.
[32] L. Wang, L. Duan, G. Liu, J. Sun, M. A. Shahbazi, S. C. Kundu, R. L. Reis, B. Xiao, X. Yang, *Adv. Sci.* **2023**, *10*, 2207352.
[33] X. Wang, Y. Guo, J. Li, M. You, Y. Yu, J. Yang, G. Qin, Q. Chen, *ACS Appl. Mater. Interfaces* **2022**, *14*, 36166.
[34] X. Zhao, H. Wu, B. Guo, R. Dong, Y. Qiu, P. X. Ma, *Biomaterials* **2017**, *122*, 34.
[35] J. Liu, M. Qu, C. Wang, Y. Xue, H. Huang, Q. Chen, W. Sun, X. Zhou, G. Xu, X. Jiang, *Small* **2022**, *18*, 2106172.
[36] B. Saleh, H. K. Dhaliwal, R. Portillo-Lara, E. Shirzaei Sani, R. Abdi, M. M. Amiji, N. Annabi, *Small* **2019**, *15*, 1902232.
[37] Q. Xu, S. A., Y. Gao, L. Guo, J. Creagh-Flynn, D. Zhou, U. Greiser, Y. Dong, F. Wang, H. Tai, W. Liu, W. Wang, W. Wang, *Acta Biomater.* **2018**, *75*, 63.
[38] X. Zhao, Y. Liang, Y. Huang, J. He, Y. Han, B. Guo, *Adv. Funct. Mater.* **2020**, *30*, 1910748.
[39] C. Ghobril, M. W. Grinstaff, *Chem. Soc. Rev.* **2015**, *44*, 1820.
[40] K. Huang, W. Liu, W. Wei, Y. Zhao, P. Zhuang, X. Wang, Y. Wang, Y. Hu, H. Dai, *ACS Nano* **2022**, *16*, 19491.
[41] D. Atila, A. Karataş, D. Keskin, A. Tezcaner, *Int. J. Biol. Macromol.* **2022**, *218*, 760.
[42] M. S. Lord, M. H. Stenzel, A. Simmons, B. K. Milthorpe, *Biomaterials* **2006**, *27*, 1341.
[43] H. Liu, X. Hu, W. Li, M. Zhu, J. Tian, L. Li, B. Luo, C. Zhou, L. Lu, *Chem. Eng. J.* **2023**, *452*, 139368.
[44] S. Cai, C. Wu, W. Yang, W. Liang, H. Yu, L. Liu, *Nanotechno. Rev.* **2020**, *9*, 971.
[45] Y. Wu, Y. Wang, C. Zheng, C. Hu, L. Yang, Q. Kong, H. Zhang, Y. Wang, *Adv. Funct. Mater.* **2023**.
[46] X. Luo, L. Zhang, Y. Luo, Z. Cai, H. Zeng, T. Wang, Z. Liu, Y. Chen, X. Sheng, A. E. d. G. Mandlate, Z. Zhou, F. Chen, L. Zheng, *Adv. Funct. Mater.* **2023**, *33*, 2214036.
[47] A. Enezy-Ulbrich, M. A., H. Malyaran, R. D. de Lange, N. Labude, R. Plum, S. Rütten, N. Terefenko, S. Wein, S. Neuss, A. Pich, *Adv. Funct. Mater.* **2020**, *30*, 2003528.
[48] Y. Liang, X. Zhao, T. Hu, B. Chen, Z. Yin, P. X. Ma, B. Guo, *Small* **2019**, *15*, 1900046.
[49] L. Mao, L. Wang, M. Zhang, M. W. Ullah, L. Liu, W. Zhao, Y. Li, A. A. Q. Ahmed, H. Cheng, Z. Shi, G. Yang, *Adv. Healthcare Mater.* **2021**, *10*, 2100402.
[50] K. Zduńska, A. Dana, A. Kolodziejczak, H. Rotsztejn, *Skin Pharmacol. Physiol.*. **2018**, *31*, 332.
[51] S. S. Biranje, J. Sun, L. Cheng, Y. Cheng, Y. Shi, S. Yu, H. Jiao, M. Zhang, X. Lu, W. Han, Q. Wang, Z. Zhang, J. Liu, *ACS Appl. Mater. Interfaces* **2022**, *14*, 3792.
[52] B. Li, H. Li, H. Chen, Y. Liu, J. Chen, Q. Feng, X. Cao, H. Dong, *Adv. Funct. Mater.* **2023**, *33*, 2302793.
[53] N. S. Muthiah Pillai, K. Eswar, S. Amirthalingam, U. Mony, P. Kerala Varma, R. Jayakumar, *ACS Appl. Bio. Mater.* **2019**, *2*, 865.
[54] X. Zhao, Q. Lang, L. Yildirimer, Z. Y. Lin, W. Cui, N. Annabi, K. W. Ng, M. R. Dokmeci, A. M. Ghaemmaghami, A. Khademhosseini, *Adv. Healthcare Mater.* **2015**, *5*, 108.
[55] X. Sun, L. Ma, X. Li, J. Wang, Y. Li, Z. Huang, *Front. Immunol.* **2022**, *13*.
[56] G. Theocharidis, H. Yuk, H. Roh, L. Wang, I. Mezghani, J. Wu, A. Kafanas, M. Contreras, B. Sumpio, Z. Li, E. Wang, L. Chen, C. F. Guo, N. Jayaswal, X.-L. Katopodi, N. Kalavros, C. S. Nabzdyk, I. S. Vlachos, A. Veves, X. Zhao, *Nat. Biomed. Eng.* **2022**, *6*, 1118.
[57] Y. Chen, A. Udduttula, X. Xie, M. Zhou, W. Sheng, F. Yu, J. Weng, D. Wang, B. Teng, G. Manivasagam, J. V. Zhang, P.-G. Ren, B. Kang, H. Zeng, *Composites, Part B* **2021**, *222*, 109057.